Journal of Applied Chemistry JAC http://chemistry.journals.semnan.ac.ir

Ultrasonic assisted removal of Ni(II) and Co(II) ions from aqueous solutions by carboxylated nanoporous graphene

Aisan Khaligh[a], Hassan Zavvar Mousavi[a,*] and Alimorad Rashidi[b]

[a]*Department of Chemistry, Semnan University, Semnan, Iran.*
[b]*Nanotechnology Research Center, Research Institute of Petroleum Industry, Tehran, Iran*.

Article history:
Received:30/May/2016
Received in revised form: 10/Jul/2016
Accepted: 25/Jul/2016

Abstract

The present study was focused on the simultaneous removal of Ni(II) and Co(II) ions from aqueous solutions by ultrasound-assisted adsorption onto carboxylated nanoporous graphene (G-COOH). Nanoporous graphene was synthesized by chemical vapor deposition method then functionalized by carboxyl groups and finally characterized using SEM, XRD, EDX, BET and FT-IR techniques. The effects of variables such as pH, sonication time, adsorbent dosage, and temperature on simultaneous removal of Ni(II) and Co(II) ions were studied and optimized. The kinetic and isotherm experiment data could be well described with the pseudo-second order kinetic model and the Langmuir isotherm model. The maximum adsorption capacity of G-COOH for Ni(II) and Co(II) ions was 94.34 mg g^{-1} and 87.72 mg g^{-1}, respectively. Thermodynamic studies indicated that the adsorption process was spontaneous and endothermic in nature.

Keywords: Ultrasonic assisted removal, Heavy metal, Carboxylated nanoporous graphene, Isotherm, Kinetic, Thermodynamic.

1. Introduction

Heavy metal pollution has become one of the most serious environmental problems today. Unlike organic wastes, heavy metals are non-biodegradable and they can be accumulated in living tissues, causing various diseases and disorders [1, 2]. Nickel, as a hazardous heavy metal is found in various industrial activities like nickel plating, colored ceramics, batteries, furnaces used to make alloys or from power plants and trash incinerators. Over-absorption of nickel may cause cancer of lungs, nose and bones, extreme weakness, dermatitis, headache, dizziness and respiratory distress [3]. Cobalt and its salts are used in nuclear medicine, enamels and semiconductors, grinding wheels, painting on glass and porcelain, hygrometers and electroplating. The effects of acute cobalt poisoning in humans are very serious, among them are asthma, damage to the heart, thyroid and liver. Cobalt may also cause mutations in living cells [4, 5]. Therefore, removal of these heavy metal ions from such industrial effluents is

*. **Corresponding Author:** *E-mail address: hzmousavi@semnan.ac.ir; Tel.: +(98)233366194*

challenging requirement to produce a safe and clean environment.

Many technologies have been developed for removal of heavy metal ions from aquatic environments, including chemical precipitation, chemical oxidation/reduction, reverse osmosis, ion exchange, electro dialysis, ultra-filtration and adsorption [6, 7]. Among them, the wide application of adsorption is emerged from advantages including simplicity, low cost, high efficiency, wide adaptability and availability of different adsorbents [8].

Ultrasound irradiation is well known to accelerate chemical process due to the phenomenon of acoustic cavitation. Recently ultrasonic assisted adsorption process has been developed to favor the kinetic of the mass-transfer process of the adsorbate to the adsorbent and to reduce the time required for adsorption [9]. The nature and properties of the adsorbent are of prime importance in this method. In practice, the main requirements for a solid sorbent are: (a) the fast and quantitative sorption and elution, (b) a high surface area and high capacity, and (c) high dispersibility in liquid samples [9].

Graphene has recently emerged as an attractive nanosorbent for removal of heavy metal ions owing to its outstanding properties like large surface area, high adsorption capacity, and good chemical and thermal stability. Graphene is a two-dimensional, one atom thick sheet of sp^2-hybridized carbon atoms arranged in a hexagonal lattice. Unlike carbon nanotubes, both sides of the planar sheets of graphene are available for molecule adsorption [10]. Herein, the development of functionalized graphene is recommended. Functionalization may further enhance the selectivity of adsorbent.

Recently, nanoporous graphene has been synthesized by chemical vapor deposition (CVD) method and successfully been applied for the sorption of crude oil and hydrocarbons from water with respect to its large specific surface area (410 $m^2\ g^{-1}$), high pore volume (1.17 $cm^3\ g^{-1}$), and small pore size [11]. The main objective of this work is to evaluate the performance of carboxylated nanoporous graphene for ultrasonic assisted removal of Ni(II) and Co(II) ions from aqueous samples. All main factors affecting the batch adsorption process were investigated and optimized. Meanwhile, behaviors and mechanisms of heavy metal ions adsorption are comprehensively explored by kinetic and isotherm models as well as thermodynamic parameters.

2. Experimental procedure

2.1. Apparatus and Characterization Methods

Heavy metals analysis was carried out using atomic absorption spectrophotometer (Alginate, model 240 AA, USA) with air-acetylene flame, under the conditions given by the manufacturer. The pH values of the solutions were measured by a digital pH meter (Metrohm, model 744, Herisau, Switzerland). A Hettich centrifuge (model EBA 20, Hittech, Germany) and an ultrasonic bath with heating system (Tecno-GAZ SPA Ultra Sonic System) were used throughout this study. The synthesized adsorbent was characterized by X-ray diffractions (PW 1840, Phillips X-ray diffractometer, Netherland) with Cu-K_α radiation source, scanning electron microscopy (SEM, Phillips, PW3710, Netherland), energy dispersive X-ray microanalyser (EDX, QuanTax 200, Rontec, Germany) which was attached to SEM, and Fourier Transform Infrared spectrophotometer (FTIR, IFS 88, Bruker Optik GmbH, Germany) using KBr pelleting method in the 4000–400 cm^{-1}. A gas adsorption analyzer (Micromeritics ASAP 2010, Cleveland, USA) was used to measure the Brunauer-Emmett-Teller (BET) surface areas. The pH_{PZC} of sorbent was determined using the known method as described previously for 0.15 g of the sample [12].

2.2. Materials

The chemical compounds and reagents used in this work were of analytical grade and purchased from Merck (Darmstadt, Germany). Stock solutions were prepared by dissolving exact amount of nitrate salts of Ni(II) and Co(II) in deionized water to the concentration of 1000 mg L^{-1}. The standard and

experimental solutions were obtained by diluting the stock solutions with deionized water. Deionized water (DI-water) obtained from a Millipore Continental Water System (Bedford, MA, USA) was used throughout this study.

2.3. Synthesis and Carboxylation of Nanoporous Graphene

Nanoporous graphene was prepared by special CVD (chemical vapor deposition) method in a catalytic basis [11]. The reaction was carried out at 900–1100 ºC for 5–30 min using methane as the carbon source and hydrogen as the carrier gas in a ratio of 4:1. The product was then stirred in 18% HCl solution and washed repeatedly with deionized water until the solution became neutral. The treated product was finally dried in oven at 100 ºC.

For carboxylation process, 1 g of the as-prepared nanoporous grapheme was mixed with a 100 mL mixture of concentrated H_2SO_4 and HNO_3 (3:1 v/v) for 3 h at 60 ºC in an ultrasonic bath (40 kHz and 100 W). After cooling to room temperature, the reaction mixture was diluted with 500 ml of deionized water and then vacuum-filtered through a filter paper (0.22 µm porosity). This washing operation is repeated until the pH of the filtrate solution became the same as deionized water pH. Finally, the G-COOH was dried in oven at 60 °C.

2.4. Batch Adsorption Procedure

Batch adsorption experiments were performed by varying initial pH, contact time, adsorbent dose and temperature. The necessary amount of G-COOH was added to 50 mL of sample solution containing 50 mg L^{-1} of Ni (II) and Co (II) at pH of 6 (from each one). Desired pH values in the sample solution were adjusted by adding negligible volumes of NaOH or HNO_3 solutions. After ultrasonication for 12 min at 25 ºC with ultrasonic water bath (40 kHz, 130 W), the mixture was filtered through a 0.22 µm filter membrane (GSWP 47, Millipore, Billerica, MA). Finally, the residual concentrations of metal ions in the filtrate were determined by F-AAS. Removal percentage and the solid phase heavy metal concentration, qe (mg g^{-1}), were calculated as:

$$\text{Removal \%} = \frac{(C_0 - C_e)}{C_0} \times 100 \quad (1); \quad q_e = \frac{(C_0 - C_e)}{M} \times V \quad (2)$$

Where C_0 and C_e are the initial and final concentrations (mg L^{-1}) of metal ions in solution phase, respectively, V is the volume of solution (L) and M is the mass of adsorbent (g). All the adsorption experiments were replicated thrice and results were averaged.

2.5. Adsorption Isotherm

Adsorption isotherms at 6 different metal ion concentrations in the range of 75-200 mg L^{-1} were studied using the same above procedure. The solution pH, contact time, sorbent amount, and temperature were adjusted in the optimum amounts obtained from batch optimization procedure, i.e., 6, 12 min, 0.12 g and 298 K, respectively.

2.6. Adsorption Kinetics

Kinetics of Ni (II) and Co (II) ions adsorption on the G-COOH were also investigated by the same above procedure using different contact times (2-12 min) at optimum amounts of pH, adsorbent dosage and temperature.

2.7. Adsorption Thermodynamics

Thermodynamic studies at different temperatures (288, 298, 308, 318, and 328 K) were carried out by adding 0.08 g of G-COOH into 50 mL of Ni (II) and Co (II) ions solution (50 mg L^{-1}). The solution pH and ultrasonication time were adjusted in 6 and 12 min, respectively.

3. Results and discussion

3.1. Characterization of Adsorbent

The SEM image of G-COOH (Figure 1) illustrates the highly porous structure of this material with pore sizes from 45 to 63 nm.

The XRD pattern of the sample is shown in Figure 2. G-COOH shows a strong and sharp (002) peak at 2θ=24.26º (corresponding to a d-spacing of 0.35 nm), which is the characteristic peak of graphene [11].

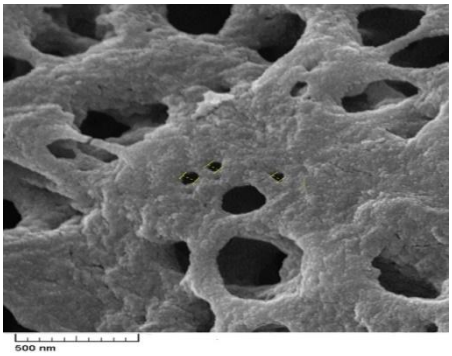

Figure 1. SEM image of carboxylated nanoporous graphene.

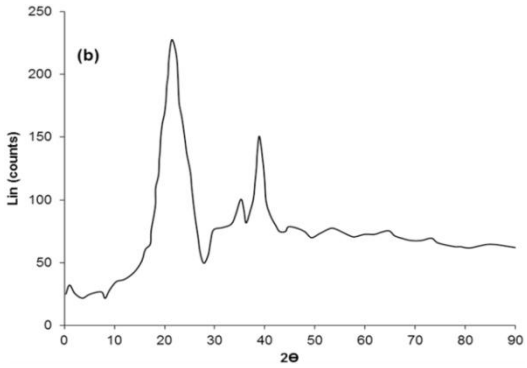

Figure 2. XRD pattern of carboxylated nanoporous graphene.

The further proofs about the functional groups are offered by the following FT-IR analysis (Figure 3). The HNO_3-H_2SO_4 treatment produced carboxyl groups on the surface of nanoporous graphene because of oxidation, as indicated by the presence of characteristic peaks at 3430 cm^{-1} and 1725 cm^{-1} for stretching vibrations of O–H and C=O of the carboxyl groups, respectively. Also, the peak at 1123 cm^{-1} is corresponded to C–O stretching vibrations of the carboxyl/or ether groups. A band at around 1630 cm^{-1} belongs to the stretching mode of the aromatic C=C double bond that forms the skeletal of the graphene sheets.

EDX data of the G-COOH was obtained and shown graphically in Figure 4. The EDX analysis of carboxylated nanoporous graphene shows high amount of element of O (22.01%) originating from oxidation of graphene.

The BET surface area of G-COOH was obtained as 320 $m^2\ g^{-1}$. Decreasing of the BET surface area in comparison with G (S_{BET}=410 $m^2\ g^{-1}$) is due to the carboxylation process.

For determination of pH_{PZC} of G and G-COOH the (pH_{final}–$pH_{initial}$) values were plotted versus their corresponding initial pH values as shown in Figure 5. It has been found that the pH_{PZC} of G is 6.3 and then, it shifts to lower pH value of 4.5 for G-COOH. These results imply that the sorbents have acidic surface since the pH_{PZC} values are less than 7.

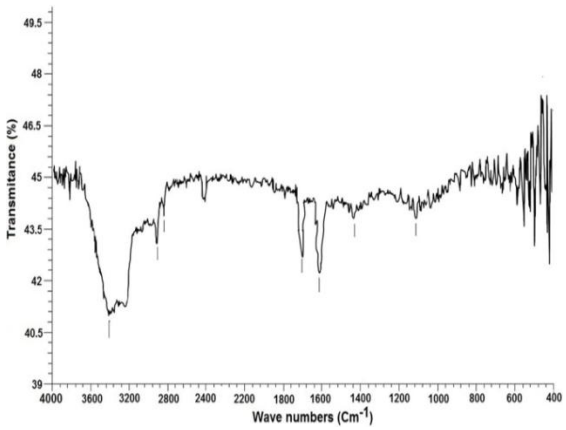

Figure 3. FT-IR spectrum of carboxylated nanoporous graphene.

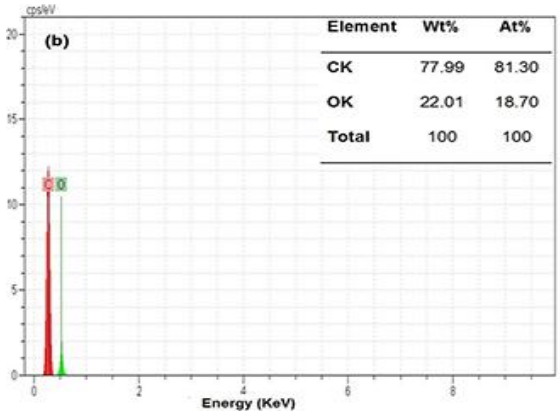

Figure 4. EDX spectrum of carboxylated nanoporous graphene.

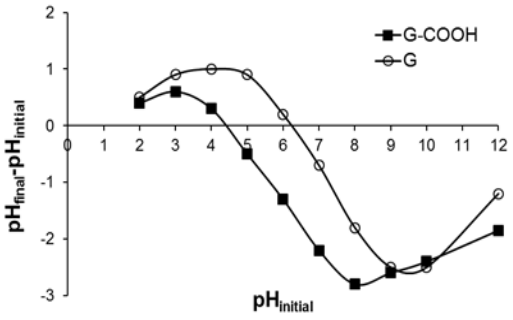

Figure 5. Final pH versus initial pH plots for 0.15 g of G and G-COOH.

3.2. Effect of pH

The effect of pH on the adsorption of Ni (II) and Co (II) ions by 0.1 g of G-COOH was studied over the pH range of 2–7.5 (to avoid metal ions precipitation), with known concentration of metal ions (50 mg L^{-1}), and ultrasonication time of 8 min at 25 ºC. As illustrated in Figure 6, removal percentage of both metal ions increased as the pH increased from 2 to 6 and then remained constant up to pH=7.5. At low pH values (pH< pH_{PZC}~4.5), solution is strongly acidic and the surface of the sorbent is surrounded by hydrogen ions and due to the competition of protons with metal ions, the removal percentages were low. At higher pH values (pH> pH_{PZC}~4.5), the sorbent surface becomes negatively charged (G-COO^-) due to the deprotonation reaction, so, the increased removal of Ni (II) and Co (II) ions is due to the strong electrostatic attraction between the sorbent surface and metal ions. Accordingly, pH=6 was chosen as the optimal pH for all further studies.

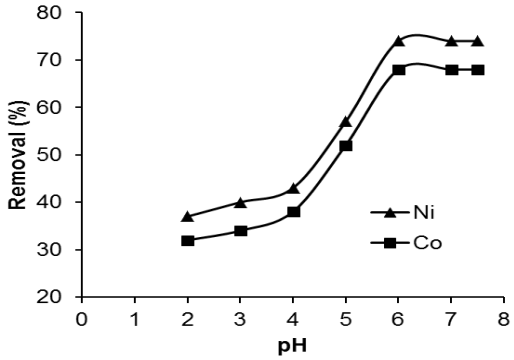

Figure 6. Effect of solution pH on adsorption of Ni(II) and Co(II) onto G-COOH (Conditions: sorbate concentration 50 mg L^{-1}; $M_{sorbent}$ 0.1 g; t=8 min; T=298 K).

3.3. Effect of Contact Time

The effect of contact time on the removal Ni (II) and Co (II) ions by G-COOH was studied using different ultrasonication times from 2 to 16 min with 50 mL of 50 mg L^{-1} metal ions solution (pH=6), and 0.1 g of G-COOH at temperature of 298 K. As can be seen from Figure 7 that the adsorption rate of metal ions onto the adsorbent was very rapid initially, which indicates that there were enough adsorption sites for the ions to be accommodated. Subsequently, the adsorption rate slowly decreased as the adsorption sites became gradually saturated, and finally it reached equilibrium in 12 min and remained constant up to 16 min. Therefore, 12 min was selected as optimum contact time for subsequent isotherm studies.

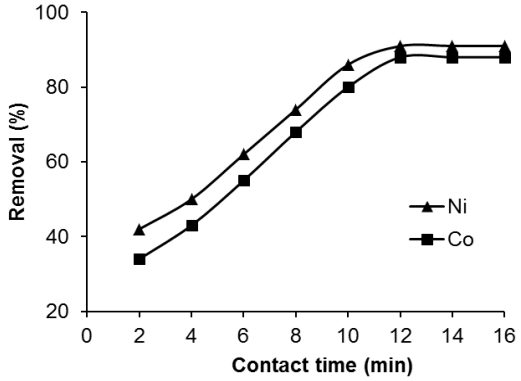

Figure 7. Effect of contact time on adsorption of Ni(II) and Co(II) onto G-COOH (Conditions: sorbate concentration 50 mg L^{-1}; pH=6; $M_{sorbent}$ 0.1 g; T=298 K).

3.4. Effect of Adsorbent dosage

Adsorption of Ni (II) and Co (II) ions was studied using different dosages of G-COOH (0.02-0.16 g) at the optimum pH and contact time. As shown in Figure 8, increase in adsorbent dosage enhanced significantly the percent removal of metal ions from aqueous solution. The maximum removal of both metal ions was obtained for the adsorbent dosage of 0.12 g. At low adsorbent dosages, the absorbent surface became saturated with the metal ions and the residual metal ion concentration in the solution was large. As the adsorbent dosage increases, the adsorbent sites available for heavy metal ions are also increased and consequently better adsorption takes place. However, higher dosages (>0.12 g) had no significant effect on the metal ions uptake as the surface metal ions concentration and the solution metal ions concentration came to equilibrium with each other. Accordingly, 0.12 of G-COOH was used in all subsequent experiments.

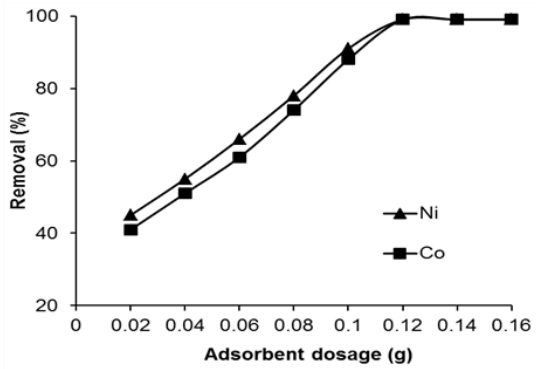

Figure 8. Effect of adsorbent dosage on adsorption of Ni(II) and Co(II) onto G-COOH (Conditions: sorbate concentration 50 mg L^{-1}; pH=6; t=12 min; T=298 K).

3.5. Effect of Temperature

The adsorption experiments of Ni (II) and Co (II) ions were performed at five different temperatures in the range of 288-328 K with 50 mL of 50 mg L^{-1} aqueous metal ions solution and 0.08 g of G-COOH at pH of 6, and contact time of 12 min. From Figure 9, the removal percentage of both metal ions by G-COOH increases with the rise in solution temperature from 288 K to 308 K, suggesting that the adsorption process is endothermic. This increase can be due to the increased mobility of metal ions and to their tendency to adsorb from the solution to the surface of the adsorbent as well as due to a greater activity of binding sites as the temperature increases.

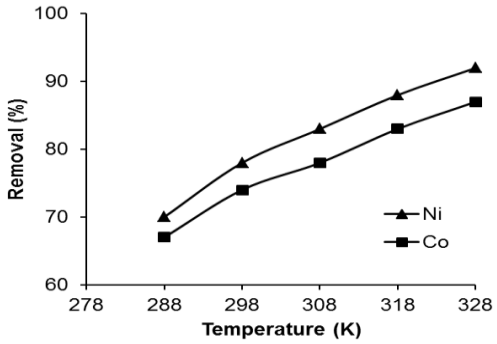

Figure 9. Effect of temperature on adsorption of Ni(II) and Co(II) onto G-COOH (Conditions: sorbate concentration 50 mg L^{-1}; pH=6; t=12 min; $M_{sorbent}$ 008 g; T=298 K).

3.6. Adsorption Isotherms

In the present work, the sorption data have been subjected to different sorption isotherms, namely, Langmuir, Freundlich and Temkin models. Langmuir adsorption isotherm is valid in the case of monolayer adsorption onto the surface with a finite number of identical sites [13]. Freundlich isotherm is used for the description of multilayer adsorption with interaction between adsorbed molecules [14]. The Temkin isotherm model assumes that the adsorption energy decreases linearly with the surface coverage due to some indirect adsorbate/adsorbate interactions [15]. The linear forms of isotherm models are defined as:

$$\frac{C_e}{q_e} = \frac{1}{K_L q_{max}} + \frac{C_e}{q_{max}} \quad (3)$$

$$\ln q_e = \ln K_F + \frac{1}{n} \ln Ce \quad (4)$$

$$q_e = B_T \ln K_T + B_T \ln Ce \quad (5)$$

The experimental equilibrium adsorption data were fitted above equations using plot of Ce/qe versus Ce, ln qe versus ln Ce, and qe versus ln Ce, respectively. Isotherm constants were determined from the slopes and intercepts of the corresponding linear plots. In Langmuir model, q_e is the amount of heavy metal ion adsorbed at equilibrium (mg g^{-1}), q_{max} is maximum adsorption capacity (mg g^{-1}) on unit mass of adsorbent, and K_L is the Langmuir constant (L mg^{-1}), related to the free energy of adsorption. Furthermore, the essential characteristic of the Langmuir isotherm, i.e., dimensionless separation factor (R_L) was calculated using Eq. (6). The R_L values between 0 and 1 indicate favorable adsorption. In Freundlich isotherm K_F and n are the isotherm constants related to adsorption capacity ($mg^{1-1/n} L^{1/n} g^{-1}$) and adsorption intensity, respectively. In Temkin model, K_T is the equilibrium binding constant (L mg^{-1}) and B_T is a constant related to adsorption heat (kJ mol^{-1}).

$$R_L = \frac{1}{1 + K_L C_0} \quad (6)$$

The results obtained by fitting the experimental equilibrium adsorption data to the isotherm models as well as the correlation coefficients (R^2) for all the models were presented in Table 1. Examination of the linear isotherm plots suggested that, for the adsorption

of metal ions onto G-COOH adsorbent, the Langmuir isotherm yielded a much better fit with higher correlation coefficient (R^2>0.99) than the other models. Also, the values of R_L are in the range of 0–1, which confirms the favorable uptake of Ni (II) and Co (II) ions by the G-COOH adsorbent. Therefore, uptake of both metal ions by G-COOH preferably followed the monolayer adsorption process.

3.7. Comparison of G-COOH-Based Batch adsorptionmethod With Others

A comparison of the maximum adsorption capacities of different adsorbents for removal of Ni(II) and Co(II) ions was also reported in Table 2. The variation in q_{max} values between the adsorbents can be related to the type and density of active sites responsible for adsorption of metal ions from the solution. It is clear from this table that the adsorption capacity of G-COOH used in the present study is significant high. This may be attributed to the effect of particle size and distribution, morphology, and surface structure of the adsorbent.

3.8. Adsorption Kinetics

In order to investigate the mechanism of metal ions adsorption on the adsorbents and examine the potential rate-controlling step, i.e., mass transfer or chemical reaction, different kinetic models were studied. The capability of Lagergren's pseudo-first-order, pseudo-second-order, and intraparticle diffusion models was examined in this study. The correlation coefficient (R^2, close or equal to 1) was introduced to evaluate the suitability of different models. The linearized-integral forms of studied kinetic models are expressed as [26-28]:

$$\ln\left(q_1 - q_t\right) = \ln q_1 - k_1 t \quad (7); \qquad \frac{t}{q_t} = \frac{1}{k_2 q_2^2} + \frac{t}{q_2} \quad (8);$$

$$q_t = k_i t^{1/2} + C_i \quad (9)$$

Table 1. Isotherm parameters for the adsorption of Ni(II) and Co (II) onto GOOH (Conditions: sorbate concentration 75-200 mg L^{-1}; $M_{sorbent}$ 0.12 g; t=12min; T=298 K).

Metal ions	Langmuir isotherm				Freundlich isotherm			Temkin isotherm		
	q_{max} (mg g^{-1})	K_L	R^2	R_L*	n	K_F	R^2	B_T	K_T	R^2
Ni(II)	94.34	0.082	0.994	0.20	2.08	13.54	0.958	22.56	1.51	0.986
Co(II)	87.72	0.076	0.995	0.21	2.22	13.14	0.984	20.36	1.54	0.989

* For C_0=50 mg L^{-1}.

Table 2. Comparison of the adsorption capacities of various adsorbents for Ni (II) and Co (II) removal by batch method.

Metal ions	Adsorbent	Adsorption capacity (mg g^{-1})		References
		Ni (II)	Co (II)	
Co (II)	Fe_3O_4/ GO	-----	22.70	[4]
Cd(II), Co (II)	Graphene oxide (GO)	-----	68.20	[16]
Ni (II)	Graphene/ MnO_2	66.00	-----	[17]
Ni (II)	Oxidized carbon nanotube	7.61	-----	[18]
Ni (II)	Ion imprinted aniline-formaldehyde polymer	71.94	-----	[19]
Ni (II)	Surface imprinted silica gel	12.61	-----	[20]
Ni(II), Cu(II) and Zn(II)	Sodium dodecyl sulphate coated Fe_3O_4	41.2	-----	[21]
Ni (II), Co (II) and Cd (II)	Eucalyptus leaves ash	23.80	27.03	[22]
Ni (II), Co (II)	Oxalate modified activated carbon	52.63	50.76	[23]
Ni (II), Co (II)	Jordan low-cost zeolite	33.00	2.73	[24]
Co (II)	Aminophosphonate chelating resin	17	8.01	[25]
Ni (II), Co (II)	Carboxylated nanoporous graphene	94.37	87.72	Present study

Where q_1 (or q_2) and q_t (mg g^{-1}) are the values of amount adsorbed per unit mass of sorbent at equilibrium and at any time t. k_1 (min^{-1}) is the pseudo-first-order adsorption rate coefficient and k_2 (g mg^{-1} min^{-1}) is the pseudo-second-order constant.

The values of k_2 were calculated from the slopes of the respective linear plots of t/q_t vs. t. In intraparticle diffusion model k_i (mg g^{-1} $min^{-1/2}$) is the diffusion rate coefficient and C_i is the intercept and relate to the thickness of the boundary layer. The parameter values for each model were obtained from the respective fitting curve resulting from the linear form of pseudo-first order, pseudo-second order and intra-particle The results along with the correlation coefficients (R^2) were listed in Table 3.

Comparing the correlation coefficients of kinetic models revealed that the pseudo-second-order kinetic model with R^2 values close to 1 matched better the experimental data than the other models.

This model is based on the assumption that the rate limiting step may be a chemical sorption involving valence forces through sharing or exchange of electrons between the adsorbent and the adsorbate [29].

3.9. Adsorption Thermodynamics

Thermodynamic studies are used to decipher any reaction in a better way. In the present study, the variation in the extent of adsorption with respect to temperature has been explained based on thermodynamic parameters viz. changes in standard free energy (ΔG^0), enthalpy (ΔH^0) and entropy (ΔS^0). Thermodynamic parameters were evaluated in the temperatures range of 288-328 K (to avoid thermal decomposition of adsorbent). The values of the thermodynamic parameters were calculated using the thermodynamic equations described below [30, 31]:

$$\Delta G^0 = -RT \ln K_C \quad (10); \qquad \ln Kc = \frac{\Delta S^0}{R} - \frac{\Delta H^0}{RT} \quad (11)$$

Table 3. Kinetic parameters for the adsorption of Ni(II) and Co (II) onto GOOH (Conditions: sorbate concentration 50 mg L^{-1}; $M_{sorbent}$ 0.12 g; t=2-10 min; T=298 K).

Metal ions	Pseudo first-order kinetic			Pseudo second-order kinetic			Intra particle diffusion		
	q_1 (mg g^{-1})	K_1	R^2	q_2 (mg g^{-1})	K_2	R^2	K_i	C_i	R^2
Ni(II)	0.267	23.57	0.987	30.12	0.006	0.997	6.509	0.968	0.991
Co(II)	0.236	22.64	0.981	30.76	0.005	0.996	6.519	1.557	0.988

Where R the ideal gas constant (8.314 J mol^{-1} K^{-1}), T is the absolute temperature (K), and Kc is the thermodynamic equilibrium constant defined by q_e/C_e. ΔH^0 and ΔS^0 values were obtained from slope and intercept of the plot ln K_c versus 1/T. The values of thermodynamic parameters thus calculated were recorded in Table 4.

Positive ΔH^0 values at different temperatures suggested the endothermic nature of adsorption process, which was in good agreement with the results that the adsorption of metal ions increased with the increasing temperature. Positive ΔS^0 values showed an increased randomness during metal ions adsorption. Negative ΔG^0 values indicated that the adsorption reaction of both metal ions was spontaneous.

Table 4. Thermodynamic parameters for the adsorption of Ni(II) and Co (II) onto GOOH (Conditions: sorbate concentration 50 mg L^{-1}; $M_{sorbent}$ 0.08 g; t=12min).

Metal ion	Parameter	Temperature (K)				
		288	298	308	318	328
Ni (II)	ΔH^0 (kJ mol^{-1})			30.70		
	ΔG^0 (kJ mol^{-1})	-3.37	-1.14	-2.28	-3.43	-4.77
	ΔS^0 (kJ $mol^{-1}K^{-1}$)			0.12		
Co (II)	ΔH^0 (kJ mol^{-1})			22.94		
	ΔG^0 (kJ mol^{-1})	-0.04	-0.87	-1.47	-2.36	-3.29
	ΔS^0 (kJ $mol^{-1}K^{-1}$)			0.08		

4. Conclusion

G-COOH was synthesized via CVD method and successfully functionalized with carboxyl groups. It was observed that the carboxylated nanoporous graphene is an efficient adsorbent for the removal of Ni(II) and Co(II) ions. The maximum removal percentage of the studied metal ions (R=99%) was obtained at optimum conditions: pH of 6, 0.12 g of sorbent, 12 min ultrasonication time, and 298 K. The isotherm models such as Langmuir, Freundlich, and Tempkin were evaluated and the equilibrium data were best described by the Langmuir model. The adsorption process was fast and pseudo-second-order rate model accurately described the kinetics of adsorption, which suggested chemisorption as the rate-limiting step in the adsorption process. Based on thermodynamic studies, the adsorption process of metal ions was both endothermic and spontaneous. Ased on the results, The proposed sorbent is useful for quantitative adsorption of Ni(II) and Co(II) ions with high sorption capacities in short time.

Acknowledgments

The authors gratefully acknowledge the financial support for this project from the Semnan University Research Council.

References

[1] S. Khan, Q. Cao, Y. Zheng, Y. Huang and Y. Zhu, *Environ. Pollut.*, 152 (2008) 686.

[2]A. Khosravi , M. Esmhosseini, S. Khezri and M. Habibimehr, *J. Applied Chem.*, 6 (2011) 61.

[3] N. Akhtar, J. Iqbal and M. Iqbal, *J. Hazard. Mater*., 108 (2004) 85.

[4] M. Liu, C. Chen, J. Hu, X. Wu and X. Wang, *The Journal of Physical Chemistry C*, 115 (2011) 25234.

[5] S. Rengaraj and S.-H. Moon, *Water Res.*, 36 (2002) 1783.

[6] F. Fu and Q. Wang, *J. Environ. Manage.*, 92 (2011) 407.

[7] M. Abedi , M. Hossien Salmani and Z. Reisi, *J. Applied Chem.*, 8 (2013) 91.

[8] S. Abedi, H. Zavvar Mousavi and A. Asghari, *Desalin. Water Treat.* (2015) 1.

[9] M. Roosta, M. Ghaedi, A. Daneshfar, R. Sahraei and A. Asghari, *Ultrason. Sonochem.*, 21 (2014) 242.

[10] H. Wang, X. Yuan, Y. Wu, H. Huang, X. Peng, G. Zeng, H. Zhong, J. Liang and M. Ren, *Adv. Colloid Interface Sci.*, 195 (2013) 19.

[11] S. Pourmand, M. Abdouss and A. Rashidi, *J. Ind. Eng. Chem.*, 22 (2015) 8.

[12] S. M. Lee and D. Tiwari, *Chem. Eng. J.*, 225 (2013) 128.

[13] I. Langmuir, *J. Am. Chem. Soc.*, 40 (1918) 1361.

[14] M. F. Hughes, B. D. Beck, Y. Chen, A. S. Lewis and D. J. Thomas, *Toxicol. Sci.*, 123 (2011) 305.

[15] M. Temkin and V. Pyzhev, *Acta Physiochim. USSR*, 12 (1940) 217.

[16] G. Zhao, J. Li, X. Ren, C. Chen and X. Wang, *Environ. Sci. Technol.*, 45 (2011) 10454.

[17] Y. Ren, N. Yan, Q. Wen, Z. Fan, T. Wei, M. Zhang and J. Ma, *Chem. Eng. J.*, 175 (2011) 1.

[18] S. Yang, J. Li, D. Shao, J. Hu and X. Wang, *J. Hazard. Mater.*, 166 (2009) 109.

[19] H. Ahmad Panahi, M. Samadi Zadeh, S. Tavangari, E. Moniri and J. Ghassemi, *Iran. J. Chem. Chem. Eng. Vol*, 31 (2012).

[20] N. Jiang, X. Chang, H. Zheng, Q. He and Z. Hu, *Anal. Chim. Acta*, 577 (2006) 225.

[21] M. Adeli, Y. Yamini and M. Faraji, *Arab. J. Chem.* (2012).

[22] H. Zavvar Mousavi and A. Khaligh, *J. Applied Chem.*, 8 (2013) 39.

[23] H. Kasaini, P. T. Kekana, A. A. Saghti and K. Bolton, *Proceedings of World Academy of Science, Engineering and Technology* (2013) 707.

[24] R. Al Dwairi and A. Al-Rawajfeh, *J. Univ. Chem. Technol. Metall.*, 47 (2012) 69.

[25] A. Deepatana and M. Valix, *J. Hazard. Mater.*, 137 (2006) 925.

[26] S. Lagergren, *Kung. Sven.Veten.Hand.*, 24 (1898) 1.

[27] Y.-S. Ho and G. McKay, *Process Biochem.*, 34 (1999) 451.

[28] W. Weber and J. Morris, *J. Sanit. Eng. Div. Am. Soc. Civ. Eng*, 89 (1963) 31.

[29] D. C. Panadare, V. G. Lade and V. K. Rathod, *Desalin. Water Treat.* (2013) 1.

[30] A. Rahmani, H. Z. Mousavi and M. Fazli, *Desalination*, 253 (2010) 94.

[31] E. Pehlivan and G. Arslan, *Fuel Process. Technol.*, 88 (2007) 99.